the rate constants, k_{ab} and k_{ba}, for equilibration of the two excited-state pentacoordinate intermediates be larger than those for the competing deactivation pathways, k_{na} and k_{nb}, i.e., have values $>10^9$ s^{-1}, a reasonable estimated lower limit for the deactivation rates.[32] In addition, it should be emphasized that the product stereochemical distribution does not simply represent the equilibrium ratio $[SP_b^*]/[SP_a^*]$ but must also include the relative k_n values, i.e.

$$\frac{\Phi_{cis}}{\Phi_{trans}} = \frac{[SP_b^*]k_{nb}}{[SP_a^*]k_{na}} = \frac{k_{ab}k_{nb}}{k_{ba}k_{na}} \quad (12)$$

Only by assuming that $k_{na} \simeq k_{nb}$ can the Φ_{cis}/Φ_{trans} product ratio be used to infer the relative energies of SP_b^* and SP_a^*.

The photochemistry of the rhodium(III) tetraammine complexes has proved very rich both in terms of photostereochemistry and in terms of ligand effects on excited-state reaction dynamics. The stereochemical lability of these complexes upon photosubstitution of a ligand clearly illustrates the difference between the photosubstitution and thermal substitution mechanisms, and consideration of the fine details provides strong circumstantial evidence for a limiting dissociative pathway as the key step of the photosubstitution mechanism. The application of pulse laser excitation techniques has allowed evaluation of the rates of the ligand substitution (dissociation) from the lowest energy (triplet) excited states of these complexes. For analogous complexes the labilization of a ligand X generally follows the order $H_2O > Cl^- > Br^- > I^-$, perhaps reflecting the relative abilities of these to π bond to an excited-state metal core with a $(d_\pi)^5(d_\sigma)^1$ configuration. Similar π-bonding considerations may explain the inverse order of these ligands in terms of the labilization rates for NH_3 loss. The stereochemical positions of these ligands also have major consequences. With regard to NH_3 substitution, most such labilization in haloammine complexes apparently occurs at a position trans to the halide. In contrast, for dihalo or aquohalo complexes, those having the cis configuration proved to have the greater ES labilities. The opposite is the case for the hydroxohalo complexes. However, both these observations are consistent with the following pattern for the cis and trans pairs $Rh(NH_3)_4XY^{n+}$: The more labile excited-state isomer in each case is also the one that undergoes the greater concomitant isomerization to the final product. A similar apparent coupling of ligand and stereochemical photolability has been reported for the isomers of dihalo trien rhodium(III) complexes.[33] Such observations may suggest some synchronous nature to the ligand dissociation and the isomerization mechanism, a possibility that is not addressed by the mode illustrated in Scheme II.[7a,8a,31] While we remain convinced that this model (or some variation upon the same theme) provides the best existing rationale for the photostereochemistry of the hexacoordinate d^6 complexes, the present excited-state kinetics data do contain clues suggesting a greater coupling of the isomerization and ligand dissociation pathways than implied by this model.

Acknowledgment. This work was supported by grants from the U.S. National Science Foundation to D.M. and to P.C.F., from NATO to L.H.S. and P.C.F., and from the Danish Natural Science Research Council and Carlsberg Foundation to L.H.S. Preliminary studies on some of these systems were carried out by Michael A. Bergkamp[18] at the UCSB laboratories. Rhodium used in these studies was provided on loan by Johnson-Matthey, Ltd.

(32) For analogous iridium(III) complexes, *cis*- and *trans*-dihalo pairs do not give common product stereochemical distributions, presumably because the higher nonradiative deactivation rates for these heavy-metal complexes are too rapid to allow full equilibration (Talebinasab-Sarvari, M.; Ford, P. C. *Inorg. Chem.* **1980**, *19*, 2640).

(33) Martins, E.; Sheridan, P. S. *Inorg. Chem.* **1978**, *17*, 2822, 3631.

Contribution from the Department of Chemistry, University of Houston, Houston, Texas 77004

Axial-Ligand-Dependent Electrochemical and Spectral Properties of a Series of Acetate- and Acetamidate-Bridged Dirhodium Complexes

MADHAV Y. CHAVAN, T. P. ZHU,[1] X. Q. LIN, M. Q. AHSAN, J. L. BEAR,* and K. M. KADISH*

Received February 24, 1984

Dirhodium complexes, $Rh_2(O_2CCH_3)_n(HNOCCH_3)_{4-n}$ and $[Rh_2(O_2CCH_3)_n(HNOCCH_3)_{4-n}]^+$ (where n = 0–4), were investigated by electrochemical and spectral techniques in nonaqueous media. A uniform variation was observed in the UV–visible spectroscopic properties and the potentials for the first oxidation of $Rh_2(O_2CCH_3)_n(HNOCCH_3)_{4-n}$ upon increasing the number of acetamidate ligands in the dimer or upon changing the nature of the axial ligand and solvent system. Electrochemical data suggest the existence of a π interaction between dirhodium centers and potential π-acceptor ligands such as Me_2SO or PPh_3. EPR spectra of the $[Rh_2(O_2CCH_3)_n(HNOCCH_3)_{4-n}]^+$ complexes suggest a change in the nature of the HOMO of the dirhodium complexes when bridging ligands are substituted for the acetates in $Rh_2(O_2CCH_3)_4$.

Introduction

The electronic structure of dirhodium tetracarboxylate complexes, $Rh_2(O_2CR)_4L_2$, has been a subject of continuing interest, particularly with respect to the nature of the metal–metal bond[2,3] and the mutual effects of metal–metal and metal–ligand interactions.[4-8] Recently, the synthesis and characterization of dirhodium(II) complexes with bridging ligands containing different kinds of donor atoms has been reported, and the electronic structure of these kinds of com-

(1) On leave from the Changchun Institute of Applied Chemistry, Academia Sinica, Changchun, Jilin, People's Republic of China.
(2) Norman, J. G., Jr.; Kolari, H. J. *J. Am. Chem. Soc.* **1978**, *100*, 791. Norman, J. G., Jr.; Renzoni, G. E.; Case, D. A. *J. Am. Chem. Soc.* **1979**, *101*, 5256.
(3) Nakatsuji, H.; Onishi, Y.; Ushio, J.; Yonezawa, T. *Inorg. Chem.* **1983**, *22*, 1623.
(4) Bursten, B. E.; Cotton, F. A. *Inorg. Chem.* **1981**, *20*, 2042.
(5) Drago, R. S.; Tanner, S. P.; Richmann, R. M.; Long, J. R. *J. Am. Chem. Soc.* **1979**, *101*, 2897.
(6) Sowa, T.; Kawamura, T.; Shida, T.; Yonezawa, T. *Inorg. Chem.* **1983**, *22*, 56.
(7) Bursten, B. E.; Christoph, G. E.; Fox, L. S., private communication, 1983.
(8) Drago, R. S.; Long, J. R.; Cosmano, R. *Inorg. Chem.* **1982**, *21*, 2196.

0020-1669/84/1323-4538$01.50/0

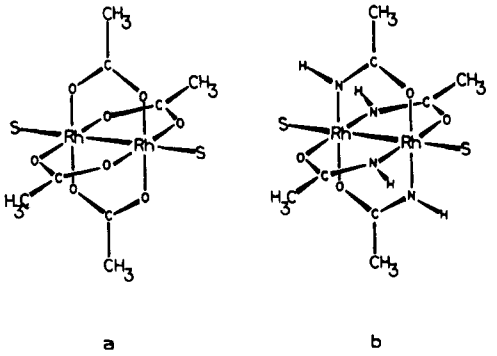

a b

Figure 1. Structures of (a) $Rh_2(ac)_4(S)_2$ and (b) $Rh_2(acam)_4(S)_2$.

pounds has been discussed.[9-15] These complexes differ substantially from the tetracarboxylates in that a large range of redox potentials are possible depending upon the specific bridging ligand.

In recent papers we have reported the synthesis and characterization of several rhodium(II) dimers with RNOCR′ bridging ligands and have shown how the oxidation potential varies as a function of the specific R and R′ group.[11-15] In the present paper we report detailed electrochemical and spectroscopic properties of dirhodium(II) complexes with acetate and acetamidate bridging ligands, $Rh_2(ac)_n(acam)_{4-n}$, where ac = $O_2CCH_3^-$, acam = $HNOCCH_3^-$, and n varies between 0 and 4. This is a continuation of an earlier work in acetonitrile[15] and describes the redox and spectroscopic properties of the complexes in four different solvent systems. These are acetonitrile, pyridine, dimethyl sulfoxide, and dichloromethane containing 0.1 M triphenylphosphine. All three neat solvents are capable of binding axially to produce the bis(ligand) adduct. The fourth solvent system generates a bis PPh_3 adduct as will be demonstrated in this paper. Both Me_2SO and PPh_3 are good π acceptors, which is not the case for acetonitrile and pyridine. Thus, this selection of solvents should provide a good basis for understanding the effect of solvent on the electrode reactions and spectroscopic properties of dirhodium acetamidates and mixed carboxylate–acetamidate systems.

Experimental Section

Chemicals. Each $Rh_2(ac)_n(acam)_{4-n}$ was synthesized by the stepwise exchange reaction of $Rh_2(ac)_4$ with acam as previously reported.[15] Five compounds were investigated in this study. These were $Rh_2(ac)_4$ (I), $Rh_2(ac)_3(acam)$ (II), $Rh_2(ac)_2(acam)_2$ (III), $Rh_2(ac)(acam)_3$ (IV), and $Rh_2(acam)_4$ (V). The structures of compounds I and V are shown in Figure 1 as bis-solvated complexes. A number of different isomers are possible for compounds III–V, but such isomers have been observed only for compound III.[15] In the present study these isomers have not been resolved, but analysis of the electrochemical data indicates little or no difference in their redox properties.[15]

Acetonitrile (CH_3CN), dimethyl sulfoxide (Me_2SO), and pyridine (py) were purchased as reagent grade from Burdick & Jackson and used without further purification. Dichloromethane (CH_2Cl_2) was purchased from Fisher Scientific Co. and was freshly distilled from CaH_2 and then P_2O_5 before use. For both electrochemical and spectroscopic experiments all solvents contained 0.1 M tetrabutylammonium perchlorate (TBAP) that was recrystallized before use.

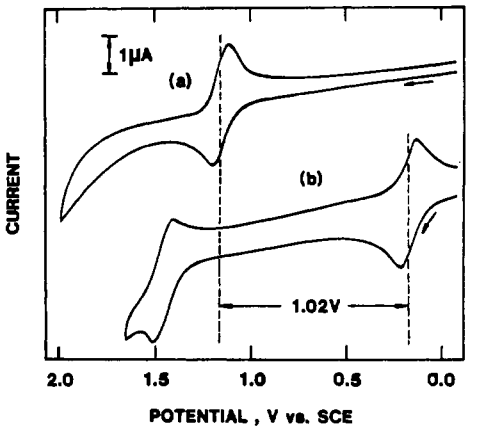

Figure 2. Cyclic voltammograms of (a) $Rh_2(ac)_4$ and (b) $Rh_2(acam)_4$ in CH_3CN, 0.1 M TBAP (scan rate 0.1 V/s).

Triphenylphosphine (PPh_3) was purchased from Aldrich Chemical Co. and was sublimed before use.

Instrumentation. Cyclic voltammetric measurements were made on Princeton Applied Research (PAR) 174 or 173/175 polarographs/potentiostats systems or an IBM EC 225 voltammetric analyzer utilizing a three-electrode system. The working electrode consisted of a platinum-button electrode. An IBM commercial satuated calomel electrode (SCE) was used as the reference electrode, and a platinum wire was used as the counterelectrode. The reference electrode was separated from the bulk of the solution by a bridge containing the same solvent and supporting electrolyte. Solutions in the bridge were changed periodically. Potentials were measured vs. SCE and were also corrected for liquid-junction potential by comparison with the ferrocene/ferrocenium couple (Fc^+/Fc) in the same solvent. Total solution volume utilized for electrochemical experiments was 5–10 mL, and the concentration of $Rh_2(ac)_n(acam)_{4-n}$ was $\sim 10^{-3}$ M.

A Cary 14-D spectrophotometer, an IBM Model 9400 spectrophotometer, or a Tracor Northern 1710 holographic optical spectrometer/multichannel analyzer was used to obtain electronic absorption spectra. No significant difference was observed between the data acquired with the three instruments. Spectroelectrochemical measurements were performed with a PAR 173/175 potentiostat coupled with a Tracor Northern 1710 holographic optical spectrometer/multichannel analyzer to obtain time-resolved spectral data. ESR spectra were measured on an IBM Model ER 100 ESR spectrometer.

Results and Discussion

Electrooxidation of $Rh_2(ac)_2(acam)_{4-n}$. Figure 2 illustrates cyclic voltammograms of $Rh_2(ac)_4$ and $Rh_2(acam)_4$ in CH_3CN (0.1 M TBAP). The electrochemistry of the former compound has been well characterized in the literature[16-19] and in 10 different solvents is reversibly oxidized according to reaction 1 or 2. In CH_3CN (0.1 M TBAP) the half-wave potential for reaction 2 is 1.17 V while in other solvent systems the range of potential for reactions 1 and 2 varies between +1.2 and +0.9 V vs. SCE.[19]

$$Rh_2(ac)_4 \rightleftarrows [Rh_2(ac)_4]^+ + e^- \quad (1)$$

$$Rh_2(ac)_4(S)_2 \rightleftarrows [Rh_2(ac)_4(S)_2]^+ + e^- \quad (2)$$

$Rh_2(acam)_4$ is not soluble in nonbonding solvents but in bonding solvents may be oxidized by two single electron-transfer reactions as represented in eq 3 and 4 where S = a

$$Rh_2(acam)_4(S)_2 \rightleftarrows [Rh_2(acam)_4(S)_2]^+ \quad (3)$$

$$[Rh_2(acam)_4(S)_2]^+ \rightleftarrows [Rh_2(acam)_4(S)_2]^{2+} \quad (4)$$

solvent molecule.[15] Both oxidations are reversible in CH_3CN

(9) Cotton, F. A.; Felthouse, T. R. *Inorg. Chem.* **1981**, *20*, 584.
(10) Tikkanen, W. R.; Binamira-Soriaga, E.; Kaska, W. C.; Ford, P. C. *Inorg. Chem.* **1983**, *22*, 1147.
(11) Dennis, A. M.; Howard, R. A.; Lançon, D.; Kadish, K. M.; Bear, J. L. *J. Chem. Soc., Chem. Commun.* **1982**, 339.
(12) Kadish, K. M.; Lancon, D.; Dennis, A. M.; Bear, J. L. *Inorg. Chem.* **1982**, *21*, 2987.
(13) Duncan, J.; Malinski, T.; Zhu, T. P.; Hu, Z. S.; Kadish, K. M.; Bear, J. L. *J. Am. Chem. Soc.* **1982**, *104*, 5507.
(14) Bear, J. L.; Zhu, T. P.; Malinski, T.; Dennis, A. M.; Kadish, K. M. *Inorg. Chem.* **1984**, *23*, 674.
(15) Zhu, T. P.; Ahsan, M. Q.; Malinski, T.; Kadish, K. M.; Bear, J. L. *Inorg. Chem.* **1984**, *23*, 2.
(16) Wilson, C. R.; Taube, H. *Inorg. Chem.* **1975**, *14*, 205.
(17) Wilson, C. R.; Taube, H. *Inorg. Chem.* **1975**, *14*, 2276.
(18) Cannon, R. D.; Powell, D. B.; Sarawek, K.; Stillman, J. S. *J. Chem. Soc., Chem. Commun.* **1976**, 31.
(19) Das, K.; Kadish, K. M.; Bear, J. L. *Inorg. Chem.* **1978**, *17*, 930.

Table I. Half-Wave Potentials for the First Oxidation of $Rh_2(ac)_n(acam)_{4-n}$ Complexes in Selected Solvents

		CH_3CN[a]		py		Me_2SO		0.1 M PPh_3 in CH_2Cl_2	
compd	formula[b]	vs. SCE	vs. Fc^+/Fc	vs. SCE	vs. Fc^+/Fc	vs. SCE	vs. Fc^+/Fc	vs. SCE	vs. Fc^+/Fc
I	$Rh_2(ac)_4(S)_2$	1.17	0.75	*c*		1.00	0.52	0.64[d]	0.14
II	$Rh_2(ac)_3(acam)(S)_2$	0.91	0.49			0.88	0.40		
III	$Rh_2(ac)_2(acam)_2(S)_2$	0.62	0.20	0.52	0.00	0.72	0.24	0.44	−0.06
IV	$Rh_2(ac)(acam)_3(S)_2$	0.37	−0.05	0.26	−0.26	0.52	0.04	0.35	−0.15
V	$Rh_2(acam)_4(S)_2$	0.15	−0.27	0.08	−0.44	0.31	−0.17	0.25	−0.25

[a] Potentials vs. SCE taken from ref 15. [b] Formula shown as bis-solvated species where S = CH_3CN, py, Me_2SO, or PPh_3. [c] Irreversible reaction reported in ref 19 at ~1.00 V. [d] A value of +0.60 has been reported in ref 26 for $Rh_2(ac)_4(PPh_3)_2$ in CH_2Cl_2.

and occur at $E_{1/2}$ = 0.15 and 1.41 V. This is shown in Figure 2b. Values of $E_{pa} - E_{pc}$ for reactions 2 and 3 vary between 60 and 70 mV at scan rates of 0.1 V/s while $i_{pa}/i_{pc} = 1$ and $i_p/v^{1/2}$ is invariant with increase in sweep rate. This indicates diffusion-controlled electron-transfer reactions in both cases. Similar reversible diffusion-controlled oxidations are observed in Me_2SO ($E_{1/2}$ = +0.31 V) and py ($E_{1/2}$ = +0.08 V), but in both solvents the second oxidation is obscured by the oxidation limit of the solvent.

For the case of $Rh_2(ac)_4$, oxidation occurs at a metal-based and not a ligand-based orbital. Both ESCA[20] and X-ray crystallography[21] give strong evidence for abstraction of half an electron from each Rh(II) center, yielding a singly charged dimeric $Rh(II^1/_2)$ complex. Similar ESCA data has been obtained for the singly oxidized $[Rh_2(acam)_4]^+$ complex and also indicates delocalization of the charge over both Rh centers, again suggesting $Rh(II^1/_2)$ formation.

The cyclic voltammograms in Figure 2 illustrate the large (1.02 V) negative shift in the first oxidation potential upon going from $Rh_2(ac)_4$ to $Rh_2(acam)_4$ in CH_3CN. This effect is clearly due to an increased electron density on the two metal centers due to the presence of the acetamidate bridging ligands in place of acetate ligands. A similar negative shift in the first oxidation potential is observed upon the stepwise substitution of acetate ligand in $Rh_2(ac)_4$ to form $Rh_2(ac)_3(acam)$, $Rh_2(ac)_2(acam)_2$, and $Rh_2(ac)(acam)_3$. This is shown in Table I, which lists $E_{1/2}$ for the first oxidation of each complex.

The linear relationship between the first oxidation potential (in CH_3CN) and the number of acetamidates on the complex is shown in Figure 3. Substitution of each acetate group by an acetamidate results in a shift of 220–290 mV in CH_3CN. Similar shifts (180–260 mV) are observed in pyridine. In contrast, a much smaller shift is observed upon changing bridging ligands in Me_2SO (120–210 mV) or CH_2Cl_2 containing 0.1 M PPh_3 (90–100 mV). This is shown in Table I and Figure 3, which displays $E_{1/2}$ vs. the number of acetamidate groups in each complex. The plots in Figure 3 show almost identical slopes in CH_3CN and py (Figure 3a). Both of these solvents have poor π-acceptor properties, which is not the case of sulfur-bound Me_2SO and CH_2Cl_2/PPh_3 solutions. In addition, it is significant to note from Figure 3a that a linear relationship is observed for CH_3CN, py, and CH_2Cl_2 containing 0.1 M PPh_3, but not for Me_2SO (Figure 3b).

In CH_3CN, the absolute potential difference for oxidation of the complexes containing 0 and 4 acetamidate groups (compounds I and V) is 1.02 V while in Me_2SO it is 0.69 V. The smallest difference occurs in CH_2Cl_2 containing PPh_3. Here the difference is only 0.39 V. This decrease in $\Delta E_{1/2}$ on going from CH_3CN to the other solvent systems suggests that the stabilizing effect of bridging ligands on dirhodium($II^1/_2$) or the destabilizing effect on dirhodium(II) is greatly dependent on the nature of the Rh–axial ligand interaction. For the specific case of the PPh_3 adducts, the effect of bridging

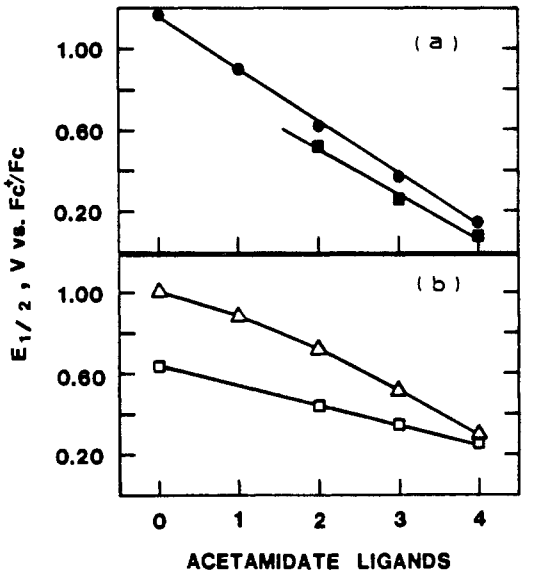

Figure 3. First oxidation potential of $Rh_2(ac)_n(acam)_{4-n}$ complexes vs. the number of acetamidate groups (4–*n*): (a) acetonitrile (●) and pyridine (■); (b) Me_2SO (△) and CH_2Cl_2, 0.1 M PPh_3 (□). All solvents contain 0.1 M TBAP.

ligands in modifying the redox potentials decreases by over 60%.

Gutmann donor numbers[22] have previously been used to correlate half-wave potentials of dirhodium carboxylates and amidates in different solvent systems.[12,14,19] For the complexes previously investigated, an increase in solvent donor number generally led to a negative (and nearly linear) shift of $E_{1/2}$. This was true for the carboxylates in all solvents[12] and for the amidates in all solvents with the exception of Me_2SO. In this solvent the potential was substantially more positive than that predicted by the simple donor number theory.[14] This same deviation occurs in this study.

The Gutmann donor number of 29.8 for Me_2SO is only valid where ligation occurs through oxygen.[22] Me_2SO is bound to the neutral compound I via a sulfur atom as evidenced by the crystal structure,[23] the S–O stretching frequencies,[24] and the characteristic orange-yellow color of sulfur-bound dirhodium carboxylates. Surprisingly, despite the fact that Me_2SO is bound via the S atom in the solid state, the $E_{1/2}$ for oxidation of $Rh_2(ac)_4S_2$ in Me_2SO solutions appears to fit the predicted donor number trend.[19] The $Rh_2(ac)_n(acam)_{4-n}$ complexes also appear to bind Me_2SO via sulfur atoms since the Me_2SO solutions are orange-yellow in color. Preliminary crystal structure investigation of the $Rh_2(ac)(acam)_3(Me_2SO)_2$ complex[25] indicates that both Me_2SO molecules are axially bound via the sulfur atoms.

(20) Dennis, A. M.; Howard, R. A.; Kadish, K. M.; Bear, J. L.; Brace, J.; Winograd, N. *Inorg. Chim. Acta* **1980**, L139.
(21) Ziolkowski, J. J.; Moszner, M.; Glowiak, T. *J. Chem. Soc., Chem. Commun.* **1977**, 760.
(22) Gutmann, V. "The Donor Acceptor Approach to Molecular Interactions"; Plenum Press: New York, 1978.
(23) Felthouse, T. R. *Prog. Inorg. Chem.* **1982**, *29*, 73 and references therein.
(24) Johnson, S. A.; Hunt, H. R.; Newman, H. M. *Inorg. Chem.* **1963**, *2*, 960.
(25) Bernal, I.; Ahsan, M. Q.; Bear, J. L., unpublished results.

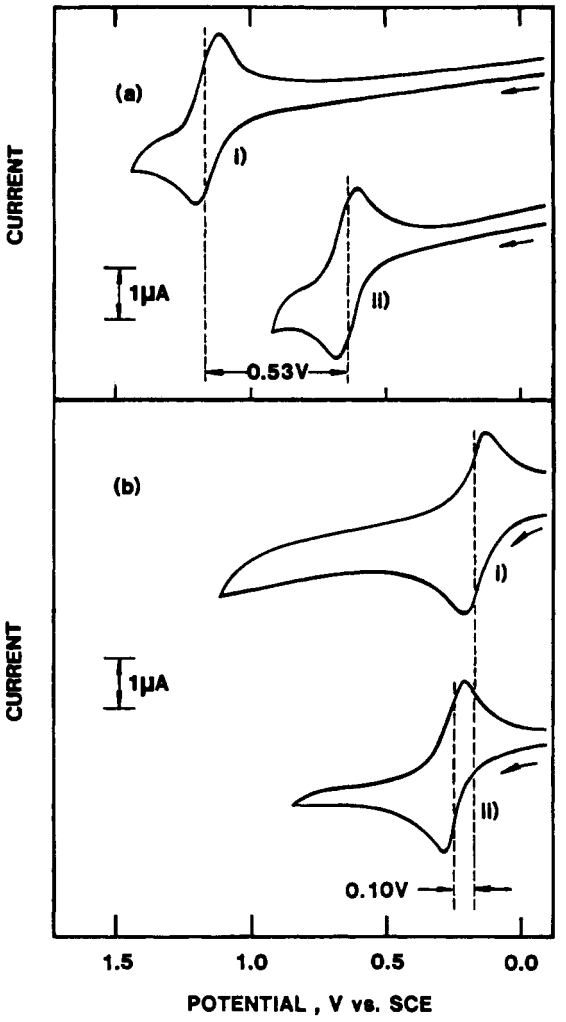

Figure 4. Cyclic voltammograms: (a) $Rh_2(ac)_4$ in (i) CH_3CN and (ii) CH_2Cl_2, 0.1 M TBAP; (b) $Rh_2(acam)_4$ in (i) CH_3CN and (ii) CH_2Cl_2 (0.1 M PPh_3).

The utilized solvents increase in donor number as follows: CH_3CN (14.1) < Me_2SO (29.8) < py (33.1).[22] Thus, on the basis of an oxidation potential of $E_{1/2}$ = −0.27 V vs. Fc^+/Fc for $Rh_2(acam)_4$ in CH_3CN and −0.44 vs. Fc^+/Fc in py, one might predict an $E_{1/2}$ for oxidation of $Rh_2(acam)_4$ in Me_2SO of about −0.40 V vs. Fc^+/Fc. The actual value is −0.17 V vs. Fc^+/Fc as seen in Table I. This $E_{1/2}$ value is 230 mV more positive than expected and reflects a relative lowering of the highest occupied molecular orbital (HOMO) from which the electron is abstracted. This suggests that the nature of the axial interaction of Me_2SO is different in the $[Rh_2(ac)_4]^{0/+}$ and $[Rh_2(acam)_4]^{0/+}$ species. The possibility of rhodium to sulfur π back-donation in the electron-rich $Rh_2(acam)_4$ complex is particularly attractive. Similar π back-bonding may occur in the other acetamidate-substituted complexes to varying degrees.

Electrochemistry in CH_2Cl_2, 0.1 M PPh_3. The electrochemistry of $Rh_2(but)_4(PPh_3)_2$, where but = butyrate, has been examined in CH_2Cl_2.[26] Addition of PPh_3 to $Rh_2(but)_4$ results in a 600-mV negative shift in $E_{1/2}$ for oxidation of the complex. A similar negative shift is observed for the oxidation of $Rh_2(ac)_4(PPh_3)_2$ as shown in Figure 4a. This compound is oxidized at a potential of 0.64 V, while $Rh_2(ac)_4(CH_3CN)_2$ is oxidized at 1.17 V. In contrast, $Rh_2(acam)_4(PPh_3)_2$ is oxidized at a more positive potential of 0.25 V, as compared to an $E_{1/2}$ = 0.15 V for $Rh_2(acam)_4(CH_3CN)_2$. This is shown in Figure 4b and illustrates the significant differences in PPh_3 interaction with compounds I and V.

(26) Kawamura, T.; Fukamachi, K.; Hayashida, S. *J. Chem. Soc., Chem. Commun.* **1979**, 945.

Table II. ESR Parameters of $[Rh_2(ac)_n(acam)_{4-n}]^+$ in Acetonitrile and Me_2SO (0.1 M TBAP)

	CH_3CN			Me_2SO			
compd	$g_\perp$, G	$g_\parallel$, G	$A_\parallel$-(Rh), 10^4 cm^{-1}	g,[a] G	$g_\perp$, G	$g_\parallel$, G	$A_\parallel$-(Rh), 10^4 cm^{-1}
I	no signal			no signal			
II	2.11[b]	1.91[b]	24.1	no signal			
III	2.11	1.92	24.1	2.16	2.11	1.91	~30
IV	2.11	1.92	26.6	2.17	2.11	1.91	~30
V	2.11	1.92	26.5	2.13	2.12	1.92/1.89	~30

[a] Additional feature; probably $g_\perp$ from another axial spectrum. [b] Additional set of complicated signals observed between $g_\perp$ and $g_\parallel$ that are not listed.

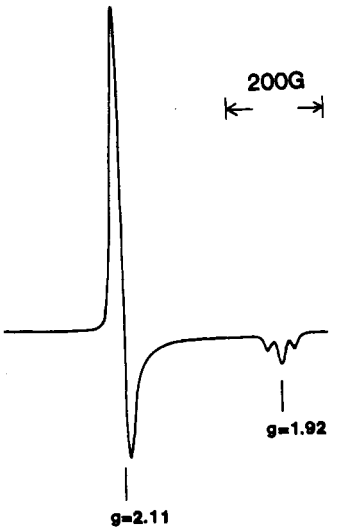

Figure 5. EPR spectrum of $[Rh_2(ac)(acam)_3]^+$ in acetonitrile (0.1 M TBAP) at 77 K.

The axial PPh_3 ligands clearly do not donate as much electron density to the $Rh_2(acam)_4$ complex as they do to $Rh_2(ac)_4$. PPh_3 is a potential π acceptor, and similar to the case of the $Rh_2(acam)_4(Me_2SO)_2$ complex, there appears to be significant π back-donation. The difference in the first oxidation potentials of the bis PPh_3 and bis CH_3CN adducts of compounds I–V decreases from −0.61 to −0.02 V vs. Fc^+/Fc as seen from Table I. Thus, it may be concluded that the extent of π back-donation increases with the number of acetamidate bridging ligands in the dimeric structure.

EPR Spectra of $[Rh_2(ac)_n(acam)_{4-n}]^+$. Each $Rh_2(ac)_n(acam)_{4-n}$ complex was oxidized under controlled potential and the resulting $[Rh_2(ac)_n(acam)_{4-n}]^+$ species investigated by EPR spectroscopy. Compounds II–V are all EPR active in the oxidized state at 77 K while compound I shows no signal in either CH_3CN or Me_2SO. None of the cationic compounds show EPR activity at room temperature in CH_3CN, Me_2SO, or CH_2Cl_2 containing 0.1 M PPh_3. The obtained EPR parameters are listed in Table II, and a representative spectrum of $[Rh_2(ac)_n(acam)_{4-n}(CH_3CN)_2]^+$ is given in Figure 5. Virtually identical spectra are observed for compounds II–V in this solvent.

The spectrum in Figure 5 shows $g_\perp$ (=2.11) > $g_\parallel$ (=1.91). The $g_\parallel$ signal is split into a triplet. The EPR spectrum of $[Rh(acam)_4]^+$ in neat pyridine (0.1 M TBAP) is virtually identical with this spectrum and has identical $g_\perp$, $g_\parallel$, and $A_\parallel$ values. The hyperfine 1:2:1 triplet in the $g_\parallel$ signal may be due

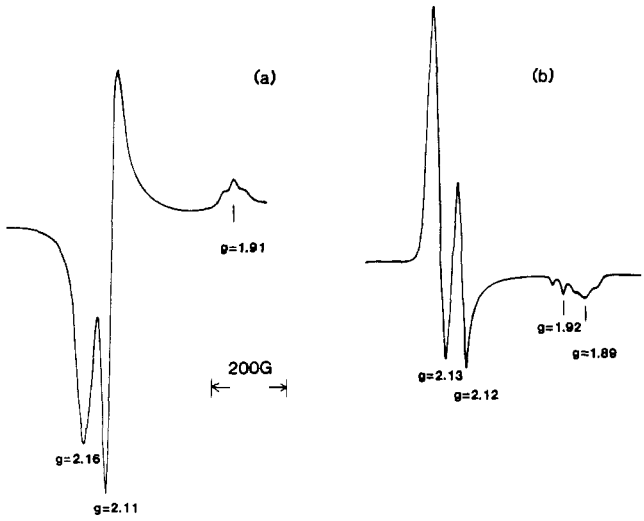

Figure 6. EPR spectra of (a) $[Rh_2(ac)_2(acam)_2]^+$ and (b) $[Rh_2(acam)_4]^+$ in Me_2SO (0.1 M TBAP) at 77 K.

to an equal interaction of the unpaired electron with two ^{103}Rh (100% abundance $I = {}^1/_2$) nuclei. There is no indication of an interaction of the unpaired electron with the nitrogen atoms ($I = 1$) of CH_3CN or py. The data on the first oxidation potential of the $Rh(ac)_n(acam)_{4-n}$ complexes, however, do indicate that CH_3CN and py interact at the axial site(s). The fact that no axial interaction is observed in the EPR spectrum may be because the unpaired electron resides in an orbital that has little or no contribution from the rhodium–solvent σ (or σ^*) orbital. However, it is quite possible that the unpaired electorn does interact with the axial nitrogen atoms, but the superhyperfine coupling cannot be seen due to the quadrupole moment of ^{14}N nuclei.

Parts a and b of Figure 6 show the EPR spectra of $[Rh_2(ac)_2(acam)_2]^+$ and $[Rh_2(acam)_4]^+$, respectively, in Me_2SO (0.1 M TBAP). The spectrum in Figure 6a appears orthorhombic, but the spectrum in Figure 6b seems to have two sets of signals with axial ($g_\perp > g_\parallel$) symmetry. It is therefore possible that the observed spectrum in Figure 6a actually consists of two sets of overlapping poorly resolved axial spectra. The $g_\parallel$ (or g_{zz}) in all cases shows hyperfine structure similar to the one observed in the CH_3CN solutions. The A value for compound IV is estimated to be 30×10^{-4} cm^{-1} and is slightly larger than that in CH_3CN and pyridine.

It is not clear why there should be two sets of axial spectra, but this might be due to two cationic species with different axial ligation involving Me_2SO. Me_2SO appears to be bonded to the Rh atoms through sulfur atoms in the neutral species. In the oxidized form, the dirhodium center must be a poorer donor of electron density (harder base than the neutral species) and may prefer bonding through oxygen to some extent. This may result in S–Rh–Rh–S, S–Rh–Rh–O, or O–Rh–Rh–O type axial ligation. The $g_\perp$ and $g_\parallel$ values for these species could differ and thus could result in the type of spectra shown in Figure 6.

The EPR spectrum of $[Rh_2(acam)_4]^+$ obtained by controlled-potential electrolysis of the neutral complex in a CH_2Cl_2 (0.1 M PPh_3) solution is shown in Figure 7. The $g_\perp$ (=2.15) is split into a triplet, and two signals at lower fields are a part of a similar triplet due to the splitting of $g_\parallel$. A part of this triplet may be buried under one of the $g_\perp$ signals at higher field. The lowest field $g_\parallel$ feature shows a superhyperfine triplet with an $A_\parallel \simeq 15 \times 10^{-4}$ cm^{-1}. Similar EPR spectra were observed by Kawamura et al.[27] in their study of the $[Rh_2(O_2CR)(PPh_3)_2]^+$ complexes. The large hyperfine splitting of $g_\perp$ and $g_\parallel$ was attributed to an interaction of the unpaired electron with two phosphorus nuclei (^{31}P, $I = {}^1/_2$), and the superhyperfine splitting of $g_\parallel$ was attributed to the interation

(27) Kawamura, T.; Fukamachi, K.; Hayashida, S.; Yonezawa, T. *J. Am. Chem. Soc.* **1981**, *103*, 364.

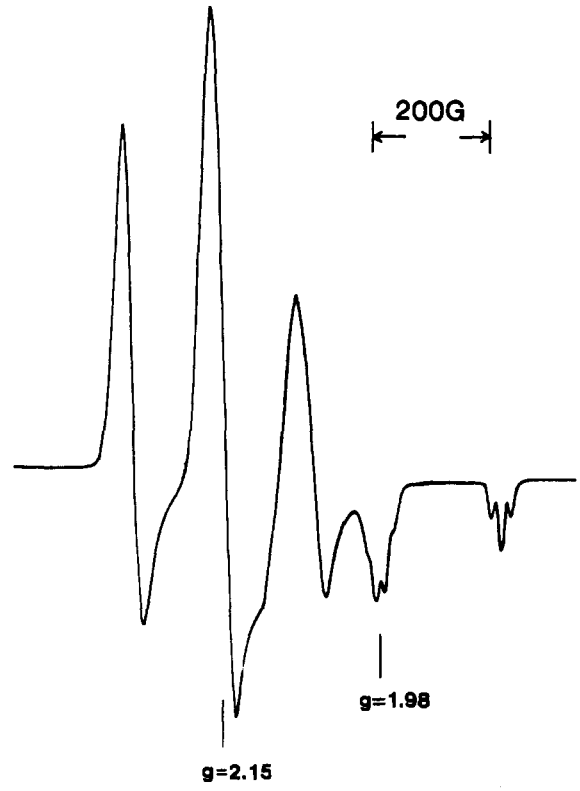

Figure 7. EPR spectrum of $[Rh_2(acam)_4]^+$ in CH_2Cl_2 (0.1 M PPh_3, 0.1 M TBAP) at 77 K.

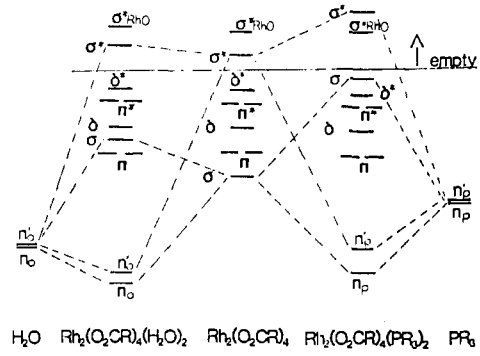

Figure 8. Relevant orbital patterns in the (a) H_2O and (b) PR_3 adducts of $Rh_2(O_2CR)_4(S)_2$ complexes (taken from ref 6).

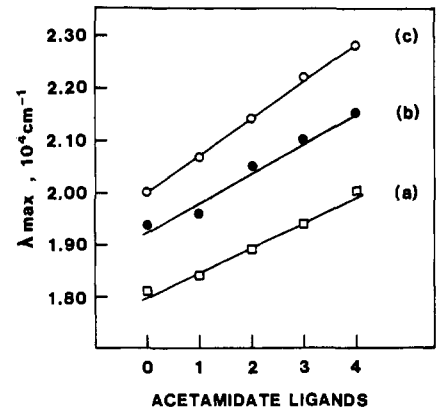

Figure 9. Plots of wavenumber of the low-energy bands of $Rh_2(ac)_n(acam)_{4-n}$ vs. the number of acetamidate ligands in the complex in CH_3CN (□), py (●), and Me_2SO (○).

Table III. Spectral Characteristics of $Rh_2(ac)_n(acam)_{4-n}$ in Selected Solvents Containing 0.1 M TBAP

compd	formula[a]	λ_{max}, nm (ϵ, 10^{-2} M^{-1} cm^{-1})		
		CH_3CN	py	Me_2SO
I	$Rh_2(ac)_4(S)_2$	552 (2.7), 427 (19)	515 (6.25), 322 (99)	500 (2.4), 304 (130)
II	$Rh_2(ac)_3(acam)(S)_2$	542 (2.2), 416 (1.7)	510 (6.1), 334 (61)	481 (3.1), 300 (200)
III	$Rh_2(ac)_2(acam)_2(S)_2$	528 (2.0), 398 (sh)	487 (2.8), 345 (50)	466 (3.4), 301 (240)
IV	$Rh_2(ac)(acam)_3(S)_2$	514 (2.0), 396 (sh), 359 (sh)	474 (4.0), 359 (60)	450 (4.4), 301 (240)
V	$Rh_2(acam)_4(S)_2$	500 (2.2), 345 (sh)	464 (sh), 389 (50)	438 (2.6), 301 (141)

[a] All complexes shown as bis-solvated species where S = CH_3CN, py, or Me_2SO.

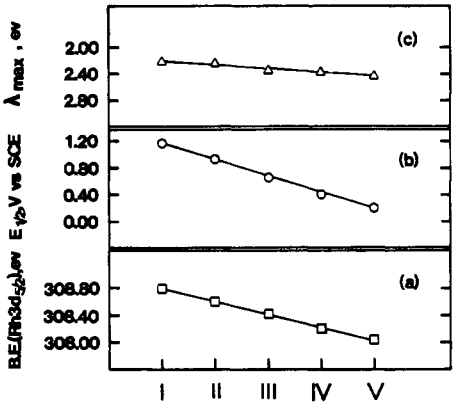

Figure 10. Plots of (a) Rh $3d_{5/2}$ binding energy, (b) first oxidation potential, and (c) energy of the low-energy band (band I) in the $Rh_2(ac)_n(acam)_{4-n}$ complexes vs. the number of acetamidates in the dimeric structure.

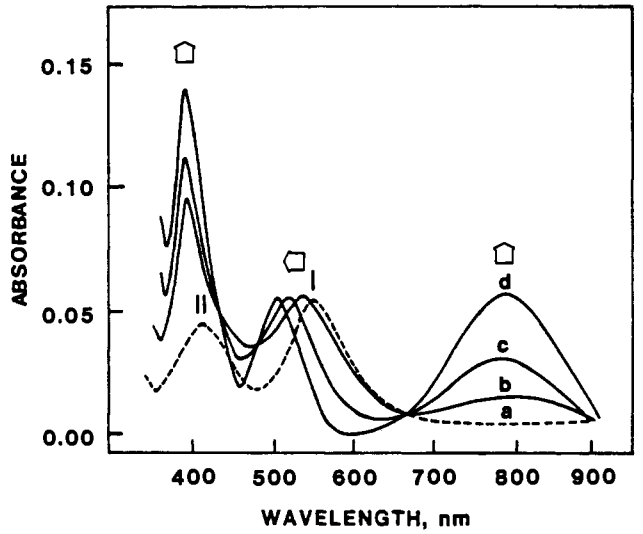

Figure 11. Time-resolved spectra for the controlled-potential oxidation of $Rh_2(ac)_4$ in CH_3CN (0.1 M TBAP). The original $Rh_2(ac)_4$ is given by (a) while (d) represents the electrogenerated $[Rh_2(ac)_4]^+$. Intermediate spectra are represented by (b) and (c).

with two ^{103}Rh nuclei. On the basis of theoretical calculations it was concluded that the HOMO in the cationic species consisted of σ_{Rh-Rh} and σ^*_{Rh-P} orbitals (Figure 8). It was argued that the energy of the p orbital of the axial phosphorus having a σ interaction with the rhodium atom was high enough to raise the σ_{Rh-Rh} orbital above the δ^* orbital. Thus, the HOMO of the cation with two axial water molecules was proposed to be different from the HOMO of the cation with two axial phosphines or phosphites.

The similarities between the EPR signal of a dirhodium carboxylate cation in the presence of PPh_3 and that of a $[Rh_2(ac)_n(acam)_{4-n}]^+$ in acetonitrile may be misleading. With weak axial ligands such as CH_3CN the orbital patterns should be more similar to those of the bis aquo adducts and not bis PR_3 adducts. In CH_3CN the $[Rh_2(ac)_4]^+$ complex (presumably $[Rh_2(ac)_4(CH_2CN)_2]^+$) does not give an EPR signal while $[Rh_2(ac)_3(acam)]^+$ gives an axial EPR signal. In a similar study,[14] a $[Rh_2(PhNOCCH_3)_4]^+$ complex was found to be EPR active even in acetone. It appears unlikely that substitution of only one acetate ligand by an acetamidate ligand can cause the HOMO to be a σ_{Rh-Rh} orbital as is suggested to be the case for the PR_3 dirhodium carboxylate complexes. On the other hand it may be argued that an important effect of substituting one acetamidate into a $Rh_2(ac)_4$ species is to destroy its symmetry. In the cationic $[Rh_2(ac)_n(acam)_{4-n}]^+$ species, this must lead to the loss of degeneracy of the π^* orbitals. If a π^* orbital is the HOMO, an unpaired electron in a nondegenerate π^* orbital may show EPR activity. Furthermore, the unpaired electron can interact equally with the two rhodium nuclei and may find itself in an axial symmetry.

Kawamura et al. have predicted[27] that an unpaired electron in the δ^*_{Rh-Rh} orbital should cause g to be $\ll 2.00$. Although our data seem to be consistent with this prediction, it may be noted that g is not affected by the number of acetamidates in the dimeric structure. This behavior appears to be inconsistent with the unpaired electron being in the δ^* orbital.[27] Further, assuming δ^* is the HOMO in the $[Rh_2(ac)_4]^+$ as well as the $[Rh_2(ac)_n(acam)_{4-n}]^+$ species, there is no apparent reason why the former should be EPR silent while the acetamidate substituted series of compounds is EPR active in CH_3CN and Me_2SO.

Electronic Absorption Spectra of $Rh_2(ac)_n(acam)_{4-n}$. The electronic absorption spectrum of $Rh_2(ac)_4$ has been well characterized in the literature.[24] Two bands are found in most solvents. The first band has been reported to range between 500 nm (Me_2SO) and 603 nm (acetone) (in the absence of supporting electrolyte) while the second band is virtually invariant with solvent and has been reported to range only between 440 and 447 nm.[24] In CH_3CN containing 0.1 M TBAP, these bands are located at 552 and 427 nm and are of approximately equal intensity.

The UV–visible spectra of the neutral dirhodium(II) carboxylates with H_2O and PR_3 axial ligands have been discussed in detail over the last few years.[2,4,6] In the case of the H_2O adducts the low-energy band had been assigned to a $\pi^*_{Rh-Rh} \rightarrow \sigma^*_{Rh-Rh}$ transition[2] but recently a $\pi^*_{Rh-Rh} \rightarrow \sigma^*_{Rh-O}$ assignment has been proposed.[28] In the case of PR_3 adducts it is assigned to a $\sigma_{Rh-Rh} \rightarrow \sigma^*_{Rh-O}$ transition.[4,6] The next higher energy band in the former case is assigned to a $\pi^*_{Rh-Rh} \rightarrow \sigma^*_{Rh-O}$ transition[2] or more recently to a $\pi_{Rh-O} \rightarrow \sigma^*_{Rh-O}$ transition[28]). For the case of PR_3 adducts it is assigned to a $\sigma_{Rh-Rh} \rightarrow \sigma^*_{Rh-Rh}$ transition. Some relevant orbital patterns are shown in Figure 8.

A single major absorption is also observed in the visible region for the partially and totally substituted $Rh_2(ac)_n(acam)_{4-n}$ complexes. This is shown in Table III, which lists all of the absorbances and the molar absorptivities in three solvent systems. As seen in this table, band I (at 552 nm in $Rh_2(ac)_4(CH_3CN)_2$ and 500 nm in $Rh_2(ac)_4(Me_2SO)_2$) undergoes a stepwise shift toward shorter wavelengths with the

(28) Miskowski, S. M.; Schaefer, W. P.; Sadeghi, B.; Santarsiero, B. D.; Gray, H. B. *Inorg. Chem.* **1984**, *23*, 1154.

Table IV. Spectral Characteristics of $[Rh_2(ac)_n(acam)_{4-n}]^+$ in CH_3CN and Me_2SO

compd	formula	λ_{max}, nm (ϵ, 10^{-2} M^{-1} cm^{-1})						
		CH_3CN			Me_2SO			
I	$[Rh_2(ac)_4]^+$	797 (2.8)	505 (2.6)	392 (4.7)	340 (4.4)	503 (0.59)	262 (260)	
II	$[Rh_2(ac)_3(acam)]^+$		520 (20)	382 (23)	209 (316)		265 (540)	
III	$[Rh_2(ac)_2(acam)_2]^+$		500 (10)	408 (21)		530 (sh)	265 (240)	
IV	$[Rh_2(ac)(acam)_3]^+$		556 (sh)	446 (49)		555 (sh)	465 (38)	296 (134)
V	$[Rh_2(acam)_4]^+$			452 (41)			458 (42)	297 (180)

sequential replacement of acetate bridging ligands. Figure 9 shows the plots of energy (cm^{-1}) of band I vs. the number of acetamidate ligands in Me_2SO, py, and CH_3CN. In all three solvents the increase in energy of band I with increase in the number of acetamidates is nearly linear.

In contrast to similar shifts of band I in all three solvents, a varied and nonconsistent behavior is observed for the higher energy band, (or shoulder) (labeled band II in Figures 11 and 12a–d). In Me_2SO, this band is independent of the number of acetamidate bridging ligands and is located at 301–304 nm.

According to the data presented by Sowa et al.[6] the $\sigma_{Rh-Rh} \rightarrow \sigma_{Rh-O}$ and $\sigma_{Rh-Rh} \rightarrow \sigma^*_{Rh-Rh}$ bands decrease in energy with increasing donor ability of the PR_3 group. The trends observed in the bis-solvated acetamidate complexes are dissimilar to those in the bis PR_3 complexes. Furthermore, the ordering of the solvent donor abilities used in this study should be $CH_3CN < Me_2SO <$ py, while the order of the energies for band I in all the compounds studied is $CH_3CN <$ py $< Me_2SO$. Thus, the transition (band I) seen in the bis-solvated species of $Rh_2(ac)_n(acam)_{4-n}$ is different from that in the bis PR_3 dirhodium carboxylates.

As mentioned earlier, band I has been assigned to a $\pi^*_{Rh-Rh} \rightarrow \sigma^*_{Rh-Rh}$ or a $\pi^*_{Rh-Rh} \rightarrow \sigma^*_{Rh-O}$ transition in the $Rh_2(O_2CR)_4$ complexes. The dependence of the energy of this transition can be explained in terms of both stabilization of the π^*_{Rh-Rh} orbital and/or the raising of the σ^*_{Rh-Rh} orbital. In either case, it appears, somewhat surprisingly, that the nature of this transition (band I) is independent of the number of acetamidates in the dirhodium complex for the following reasons: (1) The relationship between the energy of band I and the number of acetamidate ligands in compounds I–V is nearly linear in all three solvents (Figure 9). (2) The extinction coefficients of the lower energy bands in the neutral compounds I–V are nearly invariant with the type of solvent system (Table III).

Measurement of the Rh $3d_{5/2}$ binding energy of $Rh_2(ac)_n(acam)_{4-n}$ compounds shows that the molecular orbitals including the HOMO are uniformly raised upon sequential introduction of acetamidates into the dimeric structure (Figure 10). Thus, it is entirely possible that the orbital patterns do not change dramatically on going from $Rh_2(ac)_4(S)_2$ to $Rh_2(acam)_4(S)_2$. In the absence of theoretical calculations we cannot comment on the energy of the δ^* orbital in the neutral complexes. Our data suggest, however, that the orbital patterns involved in the neutral, bis-solvated $Rh_2(ac)_n(acam)_{4-n}$ complexes are more similar to those of the bis H_2O dirhodium complexes (Figure 8) than to those of the bis PR_3 dirhodium carboxylates.

Electronic Absorption Spectra of $[Rh_2(ac)_n(acam)_{4-n}]^+$. Bulk controlled-potential electrolysis and thin-layer spectroelectrochemistry were used to characterize the products of reactions 2 and 3. Upon electrochemical oxidation in CH_3CN, the bands at 552 and 427 nm shift toward higher energy while a new band appears at 797 nm. This is shown in Figure 11. Only two species are present in solution (illustrated by reaction 2) as confirmed by the presence of an isosbestic point at $\lambda \simeq$ 680 nm.

Similar oxidations were carried out for compounds II–V. Representative time-resolved spectra are given in Figure 12,

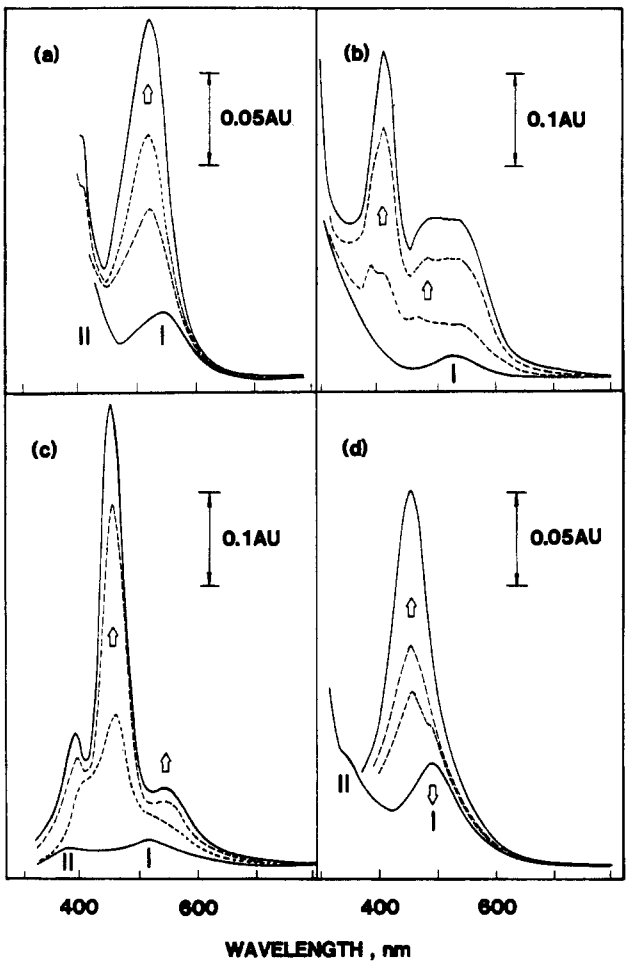

Figure 12. Time-resolved spectra for the oxidation of various $Rh_2(ac)_n(acam)_{4-n}$ complexes in CH_3CN (0.1 M TBAP): (a) $Rh_2(ac)_3(acam)$; (b) $Rh_2(ac)_2(acam)_2$; (c) $Rh_2(ac)(acam)_3$; (d) $Rh_2(acam)_4$.

and a summary of the spectral characteristics of $[Rh_2(ac)_n(acam)_{4-n}]^+$ is given in Table IV. As seen in Figure 12a,d, oxidized compounds II and V have spectra consisting of one single absorption peak between 450 and 800 nm. It may be pointed out that only one isomer is possible for compound II while only one isomer (shown in Figure 1b.) is observed for compound V. The cations of these two compounds show uncomplicated spectra (Figure 12a,d) while the cation of compound III (Figure 12b) (for which more than one isomer has been observed but not isolated) shows a complicated spectrum with additional bands between 500 and 600 nm. This might suggest that the complicated spectra are due to the presence of isomers. However, compound IV (Figure 12c) appears to have no isomers and yet also has a complicated spectrum.

The electronic absorption spectrum of the $[Rh_2(ac)_4]^+$ cation has been interpreted[2] by assigning the transitions to $\delta \rightarrow \delta^*_{Rh-Rh}$, $\pi^* \rightarrow \sigma^*_{Rh-Rh}$, and $\pi^*_{Rh-Rh} \rightarrow \sigma^*_{Rh-O}$ in increasing order of energy. The $\pi^*_{Rh-Rh} \rightarrow \sigma^*_{Rh-Rh}$ and the $\pi^*_{Rh-Rh} \rightarrow \sigma^*_{Rh-O}$ transitions occur at higher energies in the cation than in the neutral species. The EPR spectrum of $[Rh_2(ac)_4$-

$(CH_3CN)_2]^+$ illustrated in Figure 5 and Table III is consistent with the above-mentioned work.

It is difficult to make an assignment of the spectra of different $[Rh_2(ac)_n(acam)_{4-n}]^+$ cations with respect to the spectra of $[Rh_2(ac)_4]^+$. There are several distinct dissimilarities in the UV–visible spectrum of the $[Rh_2(ac)_4(CH_3CN)_2]^+$ cation and the spectra of the cations of compounds II–V. Firstly, the low-energy ($\delta \rightarrow \delta^*$) band around 800 nm is absent in the cations of compounds II–V. In addition, there is no high-intensity band in the 500-nm region for the $[Rh_2(ac)_4(CH_3CN)_2]^+$ cation.

Plots of λ_{max} for the low-energy band of oxidized compounds II–V were plotted vs. the number of acetamidate ligands. This plot is linear and when extrapolated to zero acetamidate ligands (i.e., the $[Rh_2(ac)_4]^+$ complex) in CH_3CN gives a value of $\lambda_{max} \simeq 550$ nm. This λ_{max} value may be compared to an actual absorbance of 505 nm in this solvent. These differences suggest that different orbital patterns are involved in electronic transitions of the oxidized compound I and the series of oxidized compounds II–V. This observation is consistent with the fact that the oxidized compound I is EPR silent and the oxidized compounds II–V are all EPR active (except for the oxidized compound II in Me_2SO) (Table II).

Acknowledgment. The support of the Robert A. Welch Foundation (to J.L.B., Grant E918; to K.M.K., Grant E680) is acknowledged. We also acknowledge helpful conversations with Dr. Ivan Bernal.

Registry No. TBAP, 1923-70-2; $Rh_2(ac)_4$, 15956-28-2; $Rh_2(ac)_4(CH_3CN)_2$, 80419-75-6; $Rh_2(ac)_4(py)_2$, 13987-30-9; $Rh_2(ac)_4(Me_2SO)_2$, 39773-10-9; $Rh_2(ac)_4(PPh_3)_2$, 39773-08-5; $Rh_2(ac)_4(CH_3CN)_2^+$, 92526-07-3; $Rh_2(ac)_4(Me_2SO)_2^+$, 92526-08-4; $Rh_2(ac)_3(acam)(CH_3CN)_2$, 92525-89-8; $Rh_2(ac)_3(acam)(py)_2$, 92543-06-1; $Rh_2(ac)_3(acam)(Me_2SO)_2$, 92525-94-5; $Rh_2(ac)_3(acam)(CH_3CN)_2^+$, 92526-00-6; $Rh_2(ac)_3(acam)(Me_2SO)_2^+$, 92526-09-5; $Rh_2(ac)_2(acam)_2(CH_3CN)_2$, 92525-90-1; $Rh_2(ac)_2(acam)_2(py)_2$, 92525-92-3; $Rh_2(ac)_2(acam)_2(Me_2SO)_2$, 92525-95-6; $Rh_2(ac)_2(acam)_2(PPh_3)_2$, 92525-98-9; $Rh_2(ac)_2(acam)_2(CH_3CN)_2^+$, 92526-01-7; $Rh_2(ac)_2(acam)_2(Me_2SO)_2^+$, 92526-04-0; $Rh_2(ac)(acam)_3(CH_3CN)_2$, 92525-91-2; $Rh_2(ac)(acam)_3(py)_2$, 92525-93-4; $Rh_2(ac)(acam)_3(Me_2SO)_2$, 92525-96-7; $Rh_2(ac)(acam)_3(PPh_3)_2$, 92525-99-0; $Rh_2(ac)(acam)_3(CH_3CN)_2^+$, 92526-02-8; $Rh_2(ac)(acam)_3(Me_2SO)_2^+$, 92526-05-1; $Rh_2(acam)_4(CH_3CN)_2$, 92525-88-7; $Rh_2(acam)_4(py)_2$, 90883-29-7; $Rh_2(acam)_4(Me_2SO)_2$, 92525-97-8; $Rh_2(acam)_4(PPh_3)_2$, 91837-88-6; $Rh_2(acam)_4(CH_3CN)_2^+$, 92526-03-9; $Rh_2(acam)_4(Me_2SO)_2^+$, 92526-06-2; $Rh_2(ac)_3(acam)$, 87985-37-3; $Rh_2(ac)_2(acam)_2$, 87985-38-4; $Rh_2(ac)(acam)_3$, 87985-39-5; $Rh_2(acam)_4$, 87985-40-8.

Contribution from the Departments of Chemistry, Smith College, Northampton, Massachusetts 01063, and University of California, San Diego, California 92093

Flash Photolysis of $Fe(TIM)CO(X)^{2+}$ Complexes

ALISON BUTLER[1a] and R. G. LINCK*[1b]

Received August 2, 1983

The kinetics and mechanism of substitution reactions following flash photolysis of $Fe(TIM)CO(X)^{2+}$ (X = CH_3CN, H_2O) in CO-saturated aqueous acetonitrile solutions were studied at 23 °C and at 0.5 M ionic strength. The flash forms a mixture of $Fe(TIM)(CH_3CN)_2^{2+}$, $Fe(TIM)CH_3CN(H_2O)^{2+}$, and $Fe(TIM)CO(H_2O)^{2+}$ with relative amounts depending on the $[CH_3CN]$. When $Fe(TIM)CO(X)^{2+}$ is photolyzed ($\lambda \approx 450$ nm) at $[CH_3CN] > 0.12$ M, the rate of recoordination of CO is between inverse-first and inverse-second order in $[CH_3CN]$ and first-order in both [CO] and the iron complex concentration. Below 0.12 M CH_3CN, the mechanism for CO recoordination is complicated by the rate of establishment of the equilibrium between $Fe(TIM)(CH_3CN)_2^{2+}$ and $Fe(TIM)CH_3CN(H_2O)^{2+}$, which becomes at this $[CH_3CN]$ comparable to the rate of $Fe(TIM)CO(X)^{2+}$ formation. Analysis of the mechanism of substitution shows a dramatic trans effect on the rate of water substitution by CH_3CN. When water is coordinated trans to CO, CH_3CN, and H_2O, the rates of substitution of CH_3CN for water are about 10^{-4}, 10^4, and 10^6 M^{-1} s^{-1}, respectively. Furthermore, the rate for CH_3CN loss (replacement by water) when coordinated trans to CO is 10^{-3} s^{-1}, trans to CH_3CN is 250 s^{-1}, and trans to H_2O is 10^4 s^{-1}, a 10^7 range. These trans-substitution effects are discussed in terms of the π-accepting and σ-donating abilities of the axial ligands. A previously published "solvent-sensitive" process of photolysis is analyzed in terms of these data and is shown to be caused by differential rates of reaction following photolysis.

Introduction

In a previous paper several reactions of carbon monoxide containing complexes of the macrocyclic complex of Fe(II) with 2,3,9,10-tetramethyl-1,4,8,11-tetraazacyclotetradeca-1,3,8,10-tetraene (TIM) have been reported.[2] These reactions were generally slow, on the time scale of minutes to hours. While we were investigating the properties of $Fe(TIM)CO(CH_3CN)^{2+}$, it was noted, as reported earlier, that the molecule was subject to photolysis in which CO was expelled.[3] The earlier investigators[3] interpreted their observations to imply that the *photolytic* pathway was sensitive to the solvent; in the case of $Fe(TIM)CO(CH_3CN)^{2+}$, photolysis in CH_3CN led to loss of CO and formation of $Fe(TIM)(CH_3CN)_2^{2+}$, whereas photolysis in acetone produced $Fe(TIM)CO(CH_3COCH_3)^{2+}$. Our earliest observations on the photolysis of $Fe(TIM)CO(CH_3CN)^{2+}$ in aqueous CH_3CN solutions indicated that the rate of absorbance changes after photolysis depended critically on the concentration of CH_3CN in the aqueous acetonitrile solutions. This suggests that the conclusions arrived at by Incorvia and Zink[3] may be simply a consequence of different rates of chemical reaction *following* the photolytic step. Because the kinetics of substitution of Fe(II) complexes in low-spin environments has not been well studied, and in order to probe the possibility that there is a more standard explanation for the "solvent-mediated pathway" for photolysis, we have explored the flash photolysis of $Fe(TIM)CO(CH_3CN)^{2+}$ in detail. The results of this investigation offer a rich array of interesting chemistry; they are reported herein.

Experimental Section

Synthesis and Reagents. The syntheses of the iron complexes have been described previously.[2,4] Other reagents were also subject to the procedures used previously.[2]

Flash Photolysis Procedures. All kinetic and equilibrium measurements were made at 23 °C. The ionic strength was maintained

(1) (a) University of California. (b) Smith College.
(2) Butler, A.; Linck, R. G. *Inorg. Chem.* **1984**, *23*, 2227.
(3) Incorvia, M. J.; Zink, J. I. *J. Chem. Soc., Chem. Commun.* **1977**, 730–731.
(4) Baldwin, D. A.; Pfeiffer, R. M.; Reichgott, D. W.; Rose, N. J. *J. Am. Chem. Soc.* **1973**, *95*, 5152–5158.

0020-1669/84/1323-4545$01.50/0